JACS
JOURNAL OF THE AMERICAN CHEMICAL SOCIETY
Article
Cite This: J. Am. Chem. Soc. 2019, 141, 7115−7121
pubs.acs.org/JACS

Metal−Organic Framework Photocatalyst Incorporating Bis(4′-(4-carboxyphenyl)-terpyridine)ruthenium(II) for Visible-Light-Driven Carbon Dioxide Reduction

Mahmoud Elcheikh Mahmoud,[†] Hassib Audi,[†] Abdeljalil Assoud,[‡] Tarek H. Ghaddar,*[,†] and Mohamad Hmadeh*[,†]

[†]Department of Chemistry, American University of Beirut, P.O. Box 11-0236, Riad El-Solh 1107 2020, Beirut, Lebanon
[‡]Department of Chemistry, University of Waterloo, Waterloo, Ontario, Canada, N2L 3G1

Supporting Information

ABSTRACT: In this study, we report the successful incorporation of the photoactive bis(4′-(4-carboxyphenyl)-terpyridine)ruthenium(II) ($Ru(cptpy)_2$) strut into a robust metal−organic framework (MOF), AUBM-4. The single crystal X-ray analysis revealed the formation of a new one-dimensional structure of $Ru(cptpy)_2$ complexes linked together by Zr atoms that are eight coordinated with O atoms. The chemically stable MOF structure was employed as an efficient photocatalyst for carbon dioxide conversion to formate under visible light irradiation. To the best of our knowledge, the obtained conversion rate is among the highest reported in the literature for similar systems. Our strategy of using the $Ru(cptpy)_2$ complex as a linker to construct the MOF catalyst appears to be very promising in artificial photosynthesis.

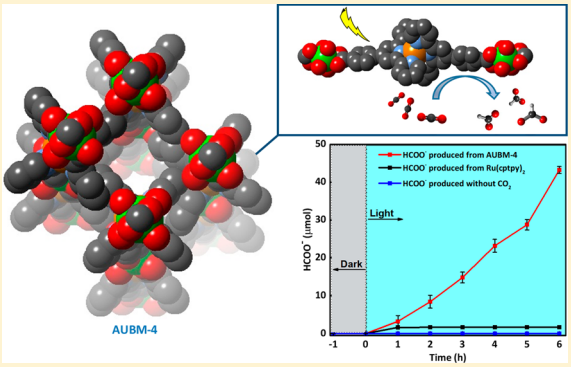

1. INTRODUCTION

Metal−organic frameworks (MOFs) are hybrid crystalline structures[1−4] that have recently emerged as promising materials in artificial photosynthesis[5] and photocatalysis.[6] Their high versatility, attributed to their synthetic tunability and exceptional structural properties, allows the incorporation of photoactive components (organo or metal-organo complexes) in the MOF's structures to enhance their photocatalytic properties.[7] Moreover, MOFs have been tested as photocatalysts for many applications, such as water oxidation,[8−10] hydrogen production,[11] carbon dioxide reduction,[12] and organic transformations,[13] where specific parts of the framework had been designed to be the catalytic center, through the metal moiety, the organic linker, molecules or both.[14] Therefore, the selection of the organic linkers and metal clusters is critical for the design and synthesis of MOF photocatalysts.[15] The integration of photoactive centers into the MOF structures can be achieved either directly[12,16] or via post-synthetic modifications,[12,17] in order to improve their photocatalytic performance as compared with their homogeneous counterparts. By tuning the functionalities on the linker, it should be possible to engineer the electronic structure of the MOF photocatalysts.[18,19] In addition, the use of MOFs in photocatalysis have been proven to be advantageous over traditional semiconductor photocatalysts due to their ability to localize electrons on distinct constituents which limits the electron−hole recombination rate.[20] Most of the reported MOF photocatalysts are based on Zr−O and Ti−O clusters[21−23] because of their high chemical stability, low toxicity, and the variable redox states of the metal center (e.g., Ti(IV)/Ti(III), Zr(IV/Zr(III)). The Zr−O and Ti−O based secondary building units (SBUs) appear as a robust platform for the construction of thermally and chemically stable MOF-based photocatalysts working under complicated and harsh catalytic conditions. The charge transfer process (e.g., LMCT) has been demonstrated for many of these MOF photocatalysts through the charge transfer from the excited ligand to Zr- or Ti-oxoclusters. In addition to metal clusters, functionalized organic linkers have been shown to contribute to the enhancement of the photocatalytic activity of the MOF catalysts.[20,24,25] In fact, the amino-modified, electron-rich conjugated, and photosensitizer-functionalized linkers have been employed in the construction of highly active MOFs[17] such as MIL-125, NH_2-UiO-66, and UiO-67 doped with photoactive complexes and porphyrin-MOFs.[26−32] The choice of these structures is due to their great visible light absorption, excess electron density, and strong interaction with CO_2 and/or water molecules. Particularly, the incorporation of Ru-polypyridine complexes (e.g., Ru(5,5′-dcbpy and Ru(4,4′-dcbpy)), in the backbone of the frameworks, has been shown to be an effective strategy to enhance the photocatalytic properties of the MOF structures[33] due to their high oxidation and reduction power and long lifetime of their excited

Received: February 26, 2019
Published: April 11, 2019

DOI: 10.1021/jacs.9b01920
J. Am. Chem. Soc. 2019, 141, 7115−7121

states.[34−36] Although the robust and highly photoactive Ru(terpyridine)$_2$ complexes and their derivatives have been widely used in homogeneous photocatalysis,[37] their integration into MOF structures to produce new photoactive materials is not well exploited.[11] Herein, we report the first structure of a photoactive Zr-MOF incorporating bis(4′-(4-carboxyphenyl)-terpyridine)Ru(II) complex (Ru(cptpy)$_2$) in its backbone (Scheme. 1). Interestingly, the obtained Zr cluster was based on the simple ZrO_8 cluster and not the conventional $Zr_6O_4(OH)_4(CO_2)_{12}$, found in UiO-66 topology. The new MOF structure was found to be highly stable and highly efficient for the visible light driven conversion of CO_2 to formate. $^{13}CO_2$ was used to confirm the origin of the formate ions produced throughout the photochemical reaction. Finally, a mechanism of the CO_2 photoreduction was discussed based on the experimental analysis and the Density Functional Theory (DFT) calculations.

Scheme 1. Synthesis of Ru(cptpy)$_2$ Linker and AUBM-4 Crystals

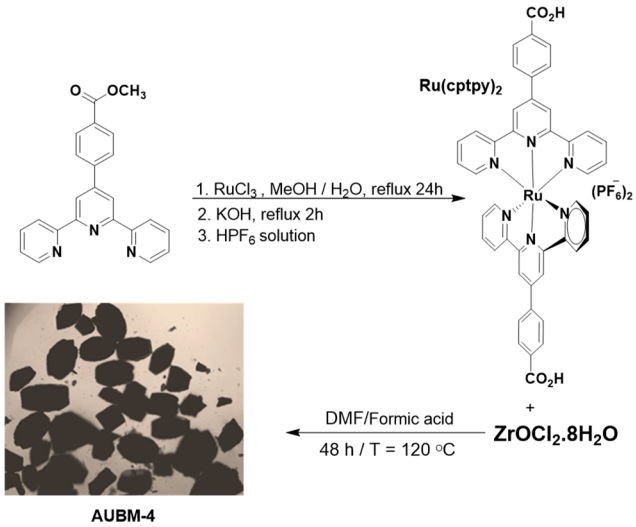

2. EXPERIMENTAL METHODS

2.1. Material and Methods. $RuCl_3·3H_2O$, 4-methoxycarbonylbenzaldehyde, 2-acethylpyridine, and all other chemicals and solvents were purchased from Sigma-Aldrich and used without any further purification. Infrared (IR) spectra were recorded on an FT-IR spectrometer Thermo-Nicolet working in the transmittance mode, in the 450−3950 cm^{-1} range. Thermogravimetric Analysis (TGA) was performed with Netzsch TG 209 F1 Libra apparatus. Powder X-ray diffraction (PXRD) patterns were collected using a Bruker D8 advance X-ray diffractometer (Bruker AXS GmbH, Karlsruhe, Germany) at 40 kV, 40 mA (1600 W) using Cu Kα radiation (k = 1.5418 Å). Absorption spectra were recorded at room temperature using a JASCOV-570 UV−vis−NIR spectrophotometer. The steady state fluorescence measurements were recorded with a resolution increment of 1 nm, slit 5 using a HORIBA Jobin Yvon Fluorolog-3 and fluorescence program. The excitation source was a 100 W xenon lamp, and the detector used was an R-928 operating at a voltage of 950 V. The formate ions were detected by 850 professional ion chromatography (Metrohm) with a Metrosep A supp 7- 250/4.0 column. NMR spectra were acquired on an AC500 Bruker spectrometer (^{1}H and ^{13}C NMR at 500 MHz). Chemical shifts were recorded in delta (δ) units and expressed as ppm values relatively to the internal standard TMS.

2.2. Synthesis of (Ru(cptpy)$_2$). 4′-(4-Methoxycarbonylphenyl)-2.2′:6′,2′′terpyridine was synthesized according to a published procedure.[38] Synthesis of the [(4′-(4-carboxylphenyl)tpy)$_2$Ru](PF$_6$)$_2$ was performed according to a modified procedure.[39] $RuCl_3·3H_2O$ (130 mg, 0.5 mmol) and 4′-(4-Methoxycarbonylphenyl)-2.2′:6′,2′′terpyridine (366 mg, 0.99 mmol) were added to a mixture of ethanol/water 1/1 (10 mL) in a round-bottom flask. The solution was refluxed overnight under an argon pressure, and then KOH (190 mg) was added and the obtained mixture was refluxed for 2 h. After cooling at room temperature, the solvents were evaporated. The crude product was washed with acetone and dissolved in few milliliters of DMF, and then ammonium hexafluorophosphate solution was added followed by HPF_6 solution. The precipitate was filtered and washed with water. Yield: 451.5 mg, 95%. Crystals of Ru(cptpy)$_2$ were produced by slow evaporation of a dimethylformamide solution of Ru(cptpy)$_2$ in the presence of urea. A summary of crystal data and refinement results is given in Table S1.

2.3. Synthesis of AUBM-4. In a 4 mL scintillation vial, 10 mg (0.01 mmol) of the complex (Ru(cptpy)$_2$) were dissolved in 2.5 mL of DMF and sonicated for 5 min, and then $ZrOCl_2·H_2O$ (30 mg, 0.09 mmol) was added. After 10 min of further sonication, 700 μL of formic acid were added and the reaction mixture was sonicated for a couple of minutes. The mixture was placed in a preheated oven at 120 °C for 48 h. Red crystals of suitable size for single X-ray analysis were obtained (yield 73% based on (Ru(cptpy)$_2$). The crystals were washed with DMF for 2 d, and the solution was exchanged with fresh DMF three times per day. This was followed by washing with acetonitrile (MeCN) for 2 d, and the solvent was exchanged with fresh MeCN three times per day. The crystals were collected and dried under dynamic vacuum at 70 °C for 6 h.

2.4. Single X-ray Analysis. The single-crystal X-ray diffraction study was performed using a Bruker Kappa Apex II CCD,[40] with Mo Kα radiation at room temperature. Several red block-like single crystals were tested, and they were heavily twinned. The best crystal was chosen for data collection using the APEX II suite search strategy by scanning $\omega-$ and ϕ in different sets of frames for full data coverage. The exposure time was 30 s per frame. The data were corrected for Lorentz and polarization effects, and a multiscan absorption correction was applied using the SADABS part of the APEX II software. The structure solution was obtained by direct method and refined using the least-square method incorporated into the SHELXTL package.[41] All the non-hydrogen atoms were refined anisotropically, and all the hydrogen atoms were refined in the idealized geometrically positions using a rigid model with C−H = 0.93 Å and isotropic displacement parameters U_{iso}(H) = 1.2U_{eq} (C). At the end of the refinement, the SQUEEZE function part of PLATON[42] program was used to check for a potential solvent accessible void by removing the electron density from a highly disordered solvent; the structure model was refined again and reached a reasonable R-value. A summary of crystal data, experimental details, and refinement results is given in Table S2.

2.5. Photocatalytic Reaction. 40 mL of acetonitrile (MeCN) and 10 mL of triethanolamine (TEOA) previously purged with argon gas were added into a 100 mL enclosed two-necked pear-shaped flask containing 20 mg of AUBM-4, and then the mixture was purged again with argon gas to remove dissolved oxygen. The mixture was placed at 20 cm irradiated with a 150 W xenon lamp through an AM 1.5 filter at room temperature with continuous stirring. After the reaction, the $HCOO^-$ ions formed were detected by 850 professional ion chromatography (Metrohm) instrument with a Metrosep A supp 7-250/4.0 column. The eluent is a solution of 3.6 mM of Na_2CO_3 and 2.5 mM HNO_3.

3. RESULTS AND DISCUSSION

3.1. Structural Characterization. The synthesis of the Ru(cptpy)$_2$ and the subsequent preparation of AUBM-4 (AUBM = American University of Beirut Materials) crystals employing this strut are summarized in Scheme 1 (NMR spectra are shown in Figures S1 and S2). Dark red crystals of Ru(cptpy)$_2$ were obtained by slow evaporation of the DMF in the presence of urea at 120 °C. The crystal structure is

DOI: 10.1021/jacs.9b01920
J. Am. Chem. Soc. 2019, 141, 7115−7121

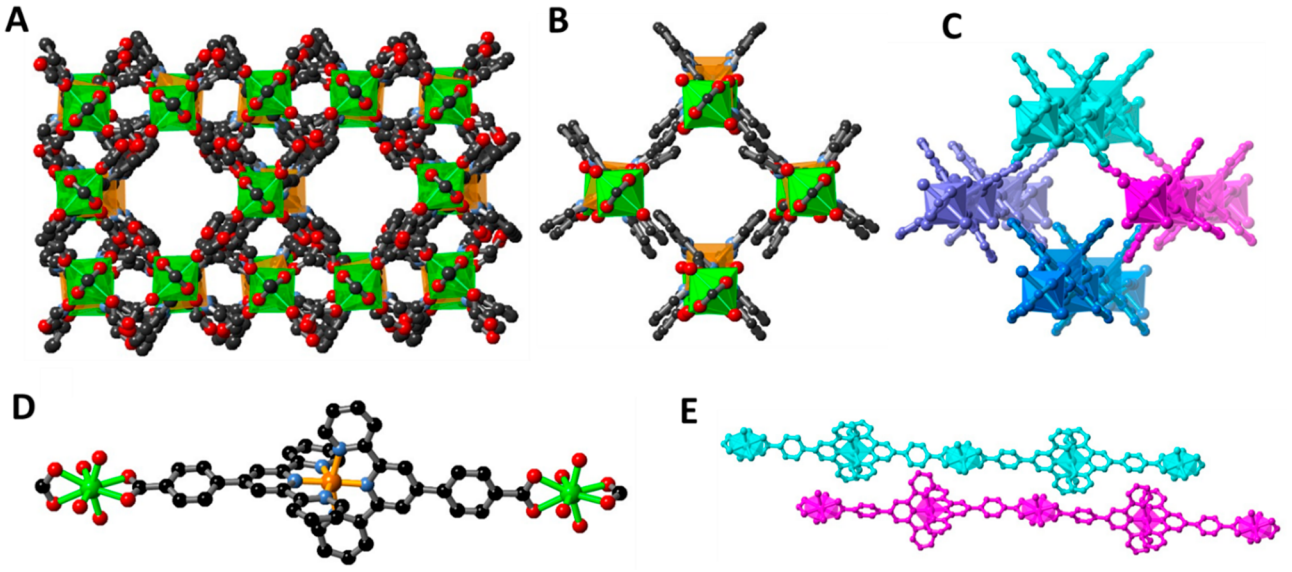

Figure 1. Crystal structure of AUBM-4: view along *x* axis (A), selected adjacent chains showing the $\pi-\pi$ interactions (B), the four chains are in different colors (C), Zr−Ru−Zr chain of AUBM-4 (color scheme: Ru, gold; Zr, green; C, black; O, red; N, blue) (D), and side view of two of the adjacent linear chains presented in cyan and turquoise (E). Hydrogen atoms are omitted for clarity.

presented in Figure S3, and the crystallographic parameters are given in Table S1. It exhibits structural parameters related to the $Ru(tpy)_2$ core that are typical of such compounds and shows that the Ru−N bonds are within the expected values with slight distortion in the N−Ru−N angles from ideal octahedral geometry. Mixing $Ru(cptpy)_2$ and $ZrOCl_2{\cdot}8H_2O$ in DMF in the presence of a small amount formic acid at 120 °C in a capped vial for 48 h resulted in the formation of red crystals of AUBM-4. The crystal structure of AUBM-4 adopts the monoclinic space group *C*2/*c* with 8 molecules per unit cell. All the atoms are located on general positions 8f except for Ru1A and Ru1B which are at Wyckoff position 4e with point symmetry 2. The crystal structure contains two crystallographically independent molecules connected through (Ru1A, Zr1A, and Ru1B) and (Ru2A, Zr2B, Ru2B, and Zr2C), respectively (Figure S4 and Table S2). These molecules form an infinite one-dimensional network along the large *a*-axis as shown in Figure 1. These infinite chains could be described as a link between the inorganic ZrO_8 secondary building units (SBUs) and the two $Ru(cptpy)_2$ complex struts, producing one-dimensional chains of Zr−$Ru(cptpy)_2$ running parallel to one another. The coordination sphere around the Zr atoms is completed by oxygen atoms from the solvent molecules to form ZrO_8 polyhedra, which are one of the five to date known Zr-based clusters in Zr-MOFs. Nevertheless, this coordination was found only in two phenolic Zr-MOFs where the polyhedra share edges to form rodlike SBUs.[43] The chains are linked together through secondary interactions such as $\pi-\pi$ interactions and hydrogen bonds.

To verify the phase purity of the AUBM-4 crystals, the powder X-ray diffraction (PXRD) pattern was recorded and compared to the simulated pattern obtained from single crystal data. As shown in Figure 2, the diffraction peaks of the as-synthesized AUBM-4 are in agreement with the simulated data, thus confirming the high crystallinity and phase purity of the MOF. This was further confirmed by the scanning electron microscopy (SEM) images and by energy-dispersive X-ray (EDX) mapping analyses which were conducted on the obtained crystals and revealed their homogeneity and the

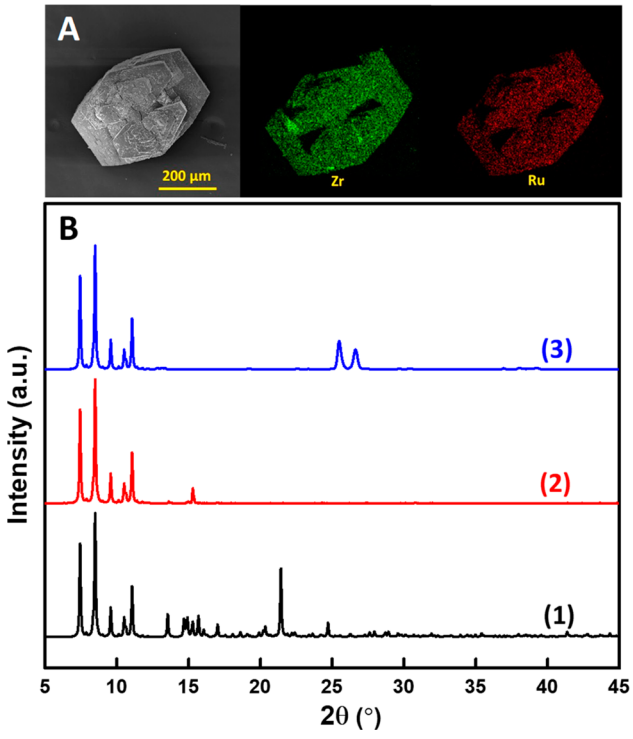

Figure 2. SEM image of AUBM-4 crystal and its mapping elements (Zr and Ru) (A); powder X-ray diffraction patterns of simulated (1), as synthesized AUBM-4 crystals (2), and after suspension in water for 1 week (3) (B).

coexistence of the elements Zr and Ru in all crystals (Figure 2 and Figure S5A). Chemical stability is of significant importance for catalysis applications, since catalysts should remain robust throughout the reaction and regeneration phases. Zr-based MOFs incorporating the octahedral and cubic clusters are reported to be highly stable; however, our AUBM-4 is composed of simple ZrO_8 cores with only two bidentate carboxylate groups and four O from the solvent, which could potentially lead to a fragile framework. Thus, we tested the

DOI: 10.1021/jacs.9b01920
J. Am. Chem. Soc. 2019, 141, 7115−7121

framework structural stability by soaking the crystals in aqueous solution and in organic solvents, for 1 week. PXRD patterns of the samples were collected after the stability test. As shown in Figure 2 and Figure S5B, the high crystallinity was retained even after soaking them in these solutions for 1 week. Although AUBM-4 is a one-dimensional structure, the packing of the chains of Zr-Ru(cptpy)$_2$ shows the existence of a porous network. In order to assess this porosity, the N_2 isotherm was performed on the activated MOF samples and the Brunauer–Emmett–Teller (BET) surface area was determined to be 50 m^2/g (Figure S6A). The thermal stability was also investigated by thermogravimetric analysis (TGA), and the weight loss profile of the activated MOF revealed several steps for the degradation of the framework starting at 300 °C where about 20% of the initial weight was lost rapidly. This was followed by two small steps of weight loss between 300 and 750 °C to reach 35% of weight loss, indicating the complete degradation of the framework (Figure S6B).

3.2. Optical Properties. To quantify the light absorption ability of AUBM-4 crystals, the diffuse reflectance of AUBM-4 powder was measured and the optical band gap was calculated to be 1.88 eV using the Tauc plot (Figure S7A). The absorption band could be attributed to the singlet metal-to-ligand charge transfer (^{1}MLCT) of ruthenium metalloligands within the MOF structure (Figure S7B). This was further observed in the luminescence spectra for both Ru(cptpy)$_2$ and AUBM-4 where the MLCT state luminescence of Ru^{2+}-based complexes was detected (Figure 3). Furthermore, the

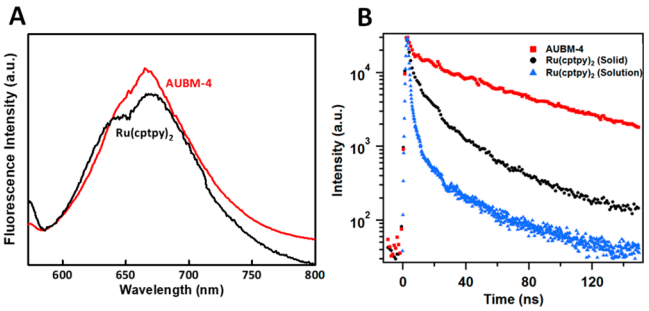

Figure 3. Photoluminescence spectra of Ru(cptpy)$_2$ and AUBM-4 (A). Time resolved luminescence traces at 520 nm of AUBM-4 crystals suspended in acetonitrile (red) and for Ru(cptpy)$_2$ suspended in chloroform (black) or dissolved in acetonitrile (blue) (B).

luminescence decays for Ru(cptpy)$_2$ and AUBM-4 show that AUBM-4 has a longer lifetime [τ = 3.6 ns (27%) and 54.1 ns (63%)] when compared to the Ru(cptpy)$_2$ complex [2.7 ns (37%) and 18.4 ns (63%)] in their solid forms.

3.3. Photocatalytic CO_2 Reduction. To evaluate the potential of AUBM-4 in photocatalytic applications, we examined its photochemical properties by visible light driven catalytic reduction of CO_2. The CO_2 photoreduction reaction was conducted using AUBM-4 crystals as a heterogeneous photocatalyst with triethanolamine (TEOA) as a sacrificial agent and acetonitrile (MeCN) as the solvent saturated with CO_2. The amount of the photocatalytic product ($HCOO^-$ anion) was quantified by ion chromatography (IC) analysis of the solution (Figure S8), and the obtained results are shown in Figure 4. The formate production increases linearly with time to reach 44 μmol in 6 h with an average formation rate of 7.3 μmol/h. Interestingly, the obtained rate was much higher than those obtained using previously reported MOF catalysts such

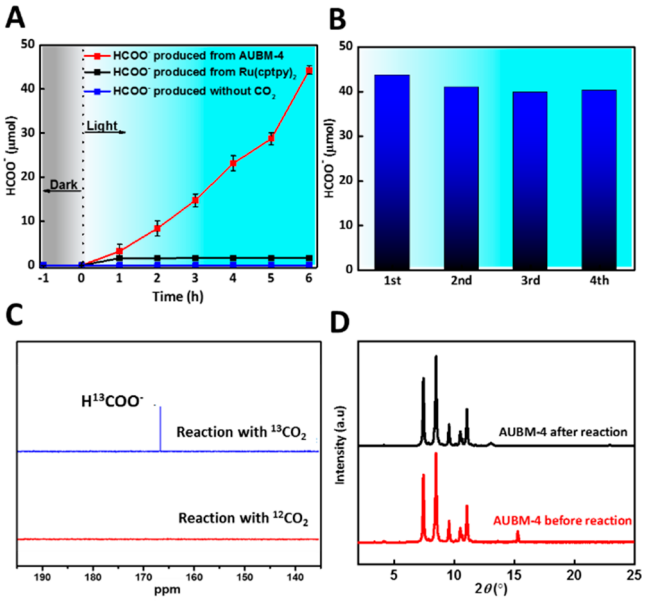

Figure 4. Amount of $HCOO^-$ generated from CO_2 as a function of the time of irradiation over AUBM-4, Ru(cptpy)$_2$, and in the absence of CO_2 source (A), recyclability of AUBM-4 photocatalyst (B), ^{13}C NMR showing the carbon source of the produced formate (C), and PXRD patterns of the catalyst recorded before and after the reaction (D).

as PCN-222, UIO-66-NH_2, and MIL-125-NH_2 under similar conditions (Table 1).[12,32,44,49]

Table 1. Conversion Rates for CO_2 Reduction to Formate Using Common MOF Photocatalysts under Similar Experimental Conditions (MeCN/TEOA)

Catalyst	Rate of $HCOO^-$ [μmol·g^{-1}·h^{-1}]	Irradiation range (nm) and Lamp intensity	ref
PCN-222	60	420–800 (300 W)	44
NH_2-UIO-66(Zr)	26.4	420–800 (500 W)	32
NH_2-MIL-53(Fe)	116.25	420–800 (300 W)	45
253-Ru(5,5′-dcbpy)$(CO)_2Cl_2$	205.8	420–800 (300 W)	46
MIL-101(Fe)	147.5	420–800 (300 W)	45
Zr-SDCA-NH_2	40.8	400–600 (300 W)	47
NNU-28	52.8	420–800 (300 W)	25
Ir-CP	158.3	420–800 (500 W)	48
Eu-Ru$(phen)_3$-MOF	94	420–800 (300 W)	12
AUBM-4	**366**	420–800 **(150 W)**	**This work**

The higher production rate was attributed to the integration of photosensitizing and light harvesting complexes in the backbone of the framework. Furthermore, a small amount of formate was produced when the linker was used as a homogeneous photocatalyst (2 μmol), while no formate was detected in the absence of catalyst, light, or CO_2. It is noteworthy that no significant amount of methane or other

DOI: 10.1021/jacs.9b01920
J. Am. Chem. Soc. 2019, 141, 7115–7121

hydrocarbon gas products were detected in the gas phase after 6 h of irradiation, as evidenced by the GC-MS analysis of the product in the head space of the reactor under our experimental conditions (Figure S9). In addition, we performed the photocatalytic production of CO_2 over AUBM-4 under a monochromatic 532 ± 5 nm light irradiation where only the ruthenium center absorbs, and again we detected the formation of formate in the solution (Figure S10). To investigate the photochemical stability of our photocatalyst, AUBM-4 was recycled and reused for four consecutive cycles, and the conversion of CO_2 to formate was monitored in each cycle. As shown in Figure 4B, there is no significant change in the amount of $HCOO^-$ anions produced from one cycle to another. Moreover, PXRD, SEM imaging, IR spectra, and BET measurements of the recycled MOF catalyst have been assessed and the results appear to be in good agreement with those of the as-synthesized sample, which demonstrates the high stability of the catalyst (Figure 4D and Figures S11–S13). The previously reported studies are interesting and informative considering the insight they provide regarding the generation of solar fuels. Unfortunately, only a small fraction of these studies have highlighted the effect of adventitious carbon contamination pervasive on the surface and the pores of these photocatalysts, which can provide false positives of their real performance metrics. The control of the reaction using $^{13}CO_2$ as a reactant was performed to verify the source of the obtained product $HCOO^-$ in our reaction. After 6 h of photocatalytic reaction, the $H^{13}COO^-$ produced was analyzed by ^{13}C NMR spectroscopy and a peak at 167.7 ppm was observed and assigned to $H^{13}COO^-$ (Figure 4C and Figures S14–S15), which clearly demonstrates that AUBM-4 is able to convert CO_2 to $HCOO^-$ through a photocatalytic reaction.

3.4. Density Functional Theory Calculations. In order to gain some insight into the mechanism of this photocatalytic reaction, we performed Density Functional Theory (DFT) calculations using the B3LYP/6-311G(d,p) exchange correlation functional with the Los Alamos effective core potential LanL2DZ[50] as implemented in the Gaussian03 program package.[51] We optimized the geometry of a small unit of AUBM-4 (without fixing atoms) containing one ruthenium and two zirconium centers in acetonitrile medium using the C-PCM algorithm[49] (Figure S16). The HOMO, HOMO−1, and HOMO−2 have a ruthenium t_{2g} character and small contribution from the π-bonding orbitals of the cptpy ligand, but with no contribution from the zirconium centers. Similarly, the LUMO to LUMO+3 are π^* orbitals delocalized on the cptpy ligands with no contribution from the zirconium units. We also performed Time-Dependent DFT calculations (TD-DFT) on the same unit in acetonitrile (Table S3 and Figures S17–S18) and showed that all transitions in the visible region (to the red of 350 nm) involve the above-mentioned molecular orbitals. These results suggest that there is no electronic transition from the ruthenium center to the zirconium ones (MMCT) upon visible light excitation as expected due to the high energy of the 4d orbitals of Zr. The lowest energy calculated for an electronic transition that involves the 4d orbitals of Zr is from the HOMO to LUMO+4, and it is calculated to be at 330 nm. These results are consistent with the emission data in Figure 3, where the emission lifetime of AUBM-4 is longer than the linker alone and therefore the MMCT is absent. These results in addition to the fact that the $Ru(cptpy)_2$ shows some CO_2 photoreduction suggest that the photocatalytic reduction reaction most probably takes place at the cptpy center. We speculate that, upon photoexcitation and the fast ruthenium-to-cptpy MLCT, the ruthenium center becomes reduced by TEOA and the $cptpy^{\bullet-}$ radical anion transfers the electron to CO_2 whether in its vicinity or coordinated to the zirconium metal, since the latter has exposed sites that can coordinate CO_2 (Scheme 2).

Scheme 2. Proposed Mechanism for CO_2 Photoreduction over AUBM-4 under Visible Light Irradiation

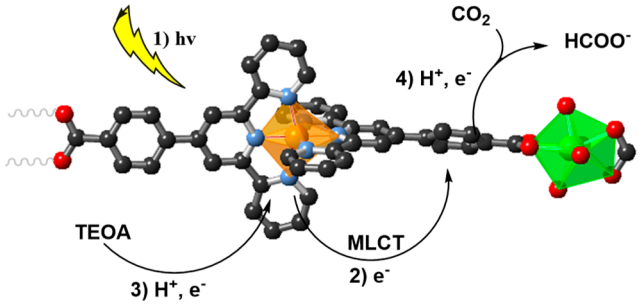

Finally, we attribute the high efficiency of this catalytic photoreduction to the following facts: (i) the long emission lifetime of the visible light harvesting $Ru(cptpy)_2$ linker in AUBM-4; (ii) the high surface that is accessible to CO_2 in AUBM-4; and (iii) the possibility of CO_2 coordinating to the zirconium center and thus facilitating the CT reaction from the terpyridine radical anion to the coordinated carbon dioxide. Even though dual mechanistic CO_2 photoreduction in MOFs at ligand and metal sites has been reported previously,[25,29] we speculate that the latter reaction is a direct reduction of coordinated carbon dioxide on the metal center by the linker radical anion rather than a reduction reaction by the metal center.

4. CONCLUSIONS

In conclusion, we have successfully synthesized and fully characterized a new chemically stable zirconium-based metal–organic framework, namely AUBM-4 assembled from a Ru metallo-ligand and ZrO_8 cluster. The AUBM-4 crystals display not only notable chemical stability but also high photostability and were employed as a photocatalyst for the reduction of carbon dioxide to formate under visible light irradiation. The obtained conversion rate (366 $\mu mol \cdot g^{-1} \cdot h^{-1}$) was among the highest reported in the literature. Recyclability of the MOF catalyst was further investigated and showed that our MOF catalyst was highly stable and was successfully regenerated. Finally, DFT calculations were performed and a mechanism for CO_2 reduction over AUBM-4 was proposed.

■ ASSOCIATED CONTENT

Supporting Information

The Supporting Information is available free of charge on the ACS Publications website at DOI: 10.1021/jacs.9b01920.

Crystallographic data for AUBM-4 (CIF)

Synthesis and characterization of the $Ru(cptpy)_2$ linker; synthesis and single X-ray details of AUBM-4 crystals in addition to SEMs, BET, TGAs, PXRDs after the chemical stability tests; details of the photocatalytic reduction of CO_2 including ^{13}C NMR and characterization of the MOF after the reaction; DFT calculations (PDF)

DOI: 10.1021/jacs.9b01920
J. Am. Chem. Soc. 2019, 141, 7115–7121

Crystallographic data for $Ru(cptpy)_2$ (CIF)

AUTHOR INFORMATION

Corresponding Authors

*tarek.ghaddar@aub.edu.lb

*mohamad.hmadeh@aub.edu.lb

ORCID

Mahmoud Elcheikh Mahmoud: 0000-0002-0990-9128

Tarek H. Ghaddar: 0000-0002-7748-0597

Mohamad Hmadeh: 0000-0003-3027-3192

Notes

The authors declare no competing financial interest.

ACKNOWLEDGMENTS

We gratefully acknowledge the funding provided by the American University of Beirut Research Board and the K. Shair Central Research Science Laboratory. M.H. acknowledges funds from The Third World Academy of Science (TWAS) Grant No. 103277. We gratefully thank Dr. Faraj Hasanayn and Mr. Mohamad Ataya for their assistance with the DFT calculations.

REFERENCES

(1) Furukawa, H.; Cordova, K. E.; O'Keeffe, M.; Yaghi, O. M. *Science* **2013**, *341* (6149), 1230444.

(2) Férey, G. *Chem. Soc. Rev.* **2008**, *37* (1), 191−214.

(3) Adil, K.; Belmabkhout, Y.; Pillai, R. S.; Cadiau, A.; Bhatt, P. M.; Assen, A. H.; Maurin, G.; Eddaoudi, M. *Chem. Soc. Rev.* **2017**, *46* (11), 3402−3430.

(4) Mason, J. A.; Veenstra, M.; Long, J. R. *Chem. Sci.* **2014**, *5* (1), 32−51.

(5) Zhang, T.; Lin, W. *Chem. Soc. Rev.* **2014**, *43* (16), 5982−5993.

(6) Diercks, C. S.; Liu, Y.; Cordova, K. E.; Yaghi, O. M. *Nat. Mater.* **2018**, *17* (4), 301−307.

(7) Li, R.; Zhang, W.; Zhou, K. *Adv. Mater.* **2018**, *30* (35), 1705512.

(8) Wang, C.; Xie, Z.; deKrafft, K. E.; Lin, W. *J. Am. Chem. Soc.* **2011**, *133* (34), 13445−13454.

(9) Xin-PingWu; Gagliardi, L.; Truhlar, D. G. *J. Chem. Phys.* **2019**, *150* (4), No. 041701.

(10) Wu, X.-P.; Gagliardi, L.; Truhlar, D. G. *J. Am. Chem. Soc.* **2018**, *140* (25), 7904−7912.

(11) Toyao, T.; Saito, M.; Dohshi, S.; Mochizuki, K.; Iwata, M.; Higashimura, H.; Horiuchi, Y.; Matsuoka, M. *Chem. Commun.* **2014**, *50* (51), 6779−6781.

(12) Yan, Z.-H.; Du, M.-H.; Liu, J.; Jin, S.; Wang, C.; Zhuang, G.-L.; Kong, X.-J.; Long, L.-S.; Zheng, L.-S. *Nat. Commun.* **2018**, *9* (1), 3353.

(13) Deng, X.; Li, Z.; García, H. *Chem. - Eur. J.* **2017**, *23* (47), 11189−11209.

(14) Yuan, S.; Qin, J.-S.; Li, J.; Huang, L.; Feng, L.; Fang, Y.; Lollar, C.; Pang, J.; Zhang, L.; Sun, D.; Alsalme, A.; Cagin, T.; Zhou, H.-C. *Nat. Commun.* **2018**, *9* (1), 808.

(15) Wang, J.-L.; Wang, C.; Lin, W. *ACS Catal.* **2012**, *2* (12), 2630−2640.

(16) Zhang, Z.-M.; Zhang, T.; Wang, C.; Lin, Z.; Long, L.-S.; Lin, W. *J. Am. Chem. Soc.* **2015**, *137* (9), 3197−3200.

(17) Cohen, S. M. *Chem. Rev.* **2012**, *112* (2), 970−1000.

(18) Hendrickx, K.; Joos, J. J.; De Vos, A.; Poelman, D.; Smet, P. F.; Van Speybroeck, V.; Van Der Voort, P.; Lejaeghere, K. *Inorg. Chem.* **2018**, *57* (9), 5463−5474.

(19) Hendrickx, K.; Vanpoucke, D. E. P.; Leus, K.; Lejaeghere, K.; Van Yperen-De Deyne, A.; Van Speybroeck, V.; Van Der Voort, P.; Hemelsoet, K. *Inorg. Chem.* **2015**, *54* (22), 10701−10710.

(20) Grau-Crespo, R.; Aziz, A.; Collins, A. W.; Crespo-Otero, R.; Hernández, N. C.; Rodriguez-Albelo, L. M.; Ruiz-Salvador, A. R.; Calero, S.; Hamad, S. *Angew. Chem., Int. Ed.* **2016**, *55* (52), 16012−16016.

(21) Yuan, S.; Qin, J.-S.; Xu, H.-Q.; Su, J.; Rossi, D.; Chen, Y.; Zhang, L.; Lollar, C.; Wang, Q.; Jiang, H.-L.; Son, D. H.; Xu, H.; Huang, Z.; Zou, X.; Zhou, H.-C. *ACS Cent. Sci.* **2018**, *4* (1), 105−111.

(22) Logan, M. W.; Ayad, S.; Adamson, J. D.; Dilbeck, T.; Hanson, K.; Uribe-Romo, F. J. *J. Mater. Chem. A* **2017**, *5* (23), 11854−11863.

(23) Nasalevich, M. A.; Hendon, C. H.; Santaclara, J. G.; Svane, K.; van der Linden, B.; Veber, S. L.; Fedin, M. V.; Houtepen, A. J.; van der Veen, M. A.; Kapteijn, F.; Walsh, A.; Gascon, J. *Sci. Rep.* **2016**, *6*, 23676.

(24) Chambers, M. B.; Wang, X.; Ellezam, L.; Ersen, O.; Fontecave, M.; Sanchez, C.; Rozes, L. *J. Am. Chem. Soc.* **2017**, *139* (24), 8222−8228.

(25) Chen, D.; Xing, H.; Wang, C.; Su, Z. *J. Mater. Chem. A* **2016**, *4* (7), 2657−2662.

(26) Huh, S.; Kim, S.-J.; Kim, Y. *CrystEngComm* **2016**, *18* (3), 345−368.

(27) Choi, K. M.; Kim, D.; Rungtaweevoranit, B.; Trickett, C. A.; Barmanbek, J. T. D.; Alshammari, A. S.; Yang, P.; Yaghi, O. M. *J. Am. Chem. Soc.* **2017**, *139* (1), 356−362.

(28) Fu, Y.; Yang, H.; Du, R.; Tu, G.; Xu, C.; Zhang, F.; Fan, M.; Zhu, W. *RSC Adv.* **2017**, *7* (68), 42819−42825.

(29) Sun, D.; Fu, Y.; Liu, W.; Ye, L.; Wang, D.; Yang, L.; Fu, X.; Li, Z. *Chem. - Eur. J.* **2013**, *19* (42), 14279−85.

(30) Hassan, G. F.; El Hoda Saad, N.; Hmadeh, M.; Karam, P. *Dalton Trans.* **2018**, *47* (44), 15765−15771.

(31) Majewski, M. B.; Peters, A. W.; Wasielewski, M. R.; Hupp, J. T.; Farha, O. K. *ACS Energy Lett.* **2018**, *3* (3), 598−611.

(32) Sun, D.; Fu, Y.; Liu, W.; Ye, L.; Wang, D.; Yang, L.; Fu, X.; Li, Z. *Chem. - Eur. J.* **2013**, *19* (42), 14279−14285.

(33) Hou, C.-C.; Li, T.-T.; Cao, S.; Chen, Y.; Fu, W.-F. *J. Mater. Chem. A* **2015**, *3* (19), 10386−10394.

(34) Cai, M.; Loague, Q. R.; Zhu, J.; Lin, S.; Usov, P. M.; Morris, A. J. *Dalton Trans.* **2018**, *47* (46), 16807−16812.

(35) Lan, G.; Li, Z.; Veroneau, S. S.; Zhu, Y.-Y.; Xu, Z.; Wang, C.; Lin, W. *J. Am. Chem. Soc.* **2018**, *140* (39), 12369−12373.

(36) Liao, W.-M.; Zhang, J.-H.; Wang, Z.; Yin, S.-Y.; Pan, M.; Wang, H.-P.; Su, C.-Y. *J. Mater. Chem. A* **2018**, *6* (24), 11337−11345.

(37) Lv, H.; Rudd, J. A.; Zhuk, P. F.; Lee, J. Y.; Constable, E. C.; Housecroft, C. E.; Hill, C. L.; Musaev, D. G.; Geletii, Y. V. *RSC Adv.* **2013**, *3* (43), 20647−20654.

(38) Constable, E. C.; Dunphy, E. L.; Housecroft, C. E.; Neuburger, M.; Schaffner, S.; Schaper, F.; Batten, S. R. *Dalton trans.* **2007**, No. 38, 4323−32.

(39) Cooke, M. W.; Tremblay, P.; Hanan, G. S. *Inorg. Chim. Acta* **2008**, *361* (8), 2259−2269.

(40) Assoud, A.; Guo, Q.; Sankar, C. R.; Kleinke, H. *Inorg. Chem. Front.* **2017**, *4* (2), 315−323.

(41) Sheldrick, G. *Acta Crystallogr., Sect. C: Struct. Chem.* **2015**, *71* (1), 3−8.

(42) Spek, A. *Acta Crystallogr., Sect. C: Struct. Chem.* **2015**, *71* (1), 9−18.

(43) Bai, Y.; Dou, Y.; Xie, L.-H.; Rutledge, W.; Li, J.-R.; Zhou, H.-C. *Chem. Soc. Rev.* **2016**, *45* (8), 2327−2367.

(44) Xu, H.-Q.; Hu, J.; Wang, D.; Li, Z.; Zhang, Q.; Luo, Y.; Yu, S.-H.; Jiang, H.-L. *J. Am. Chem. Soc.* **2015**, *137* (42), 13440−13443.

(45) Wang, D.; Huang, R.; Liu, W.; Sun, D.; Li, Z. *ACS Catal.* **2014**, *4* (12), 4254−4260.

(46) Sun, D.; Gao, Y.; Fu, J.; Zeng, X.; Chen, Z.; Li, Z. *Chem. Commun.* **2015**, *51* (13), 2645−2648.

(47) Sun, M.; Yan, S.; Sun, Y.; Yang, X.; Guo, Z.; Du, J.; Chen, D.; Chen, P.; Xing, H. *Dalton Trans.* **2018**, *47* (3), 909−915.

(48) Li, L.; Zhang, S.; Xu, L.; Wang, J.; Shi, L.-X.; Chen, Z.-N.; Hong, M.; Luo, J. *Chem. Sci.* **2014**, *5* (10), 3808−3813.

(49) Fu, Y.; Sun, D.; Chen, Y.; Huang, R.; Ding, Z.; Fu, X.; Li, Z. *Angew. Chem., Int. Ed.* **2012**, *51* (14), 3364−7.

(50) Hay, P. J.; Wadt, W. R. *J. Chem. Phys.* **1985**, *82* (1), 270−283.

DOI: 10.1021/jacs.9b01920
J. Am. Chem. Soc. 2019, 141, 7115−7121

(51) Xu, H. Q.; Hu, J.; Wang, D.; Li, Z.; Zhang, Q.; Luo, Y.; Yu, S. H.; Jiang, H. L. *J. Am. Chem. Soc.* **2015**, *137* (42), 13440−13443.

DOI: 10.1021/jacs.9b01920
J. Am. Chem. Soc. 2019, 141, 7115−7121